Article

Coordination-Based Gold Nanoparticle Layers

Meni Wanunu, Ronit Popovitz-Biro, Hagai Cohen, Alexander Vaskevich, and Israel Rubinstein

J. Am. Chem. Soc., **2005**, 127 (25), 9207-9215• DOI: 10.1021/ja050016v • Publication Date (Web): 03 June 2005

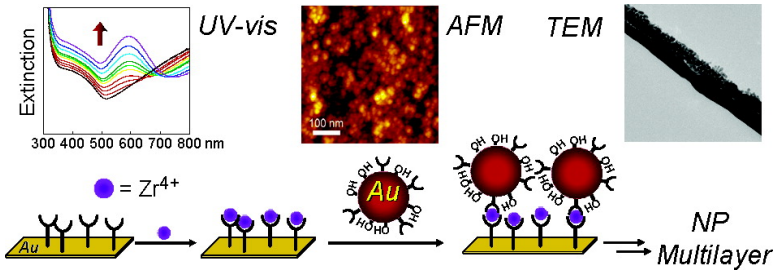

More About This Article

Additional resources and features associated with this article are available within the HTML version:

- Supporting Information
- Links to the 13 articles that cite this article, as of the time of this article download
- Access to high resolution figures
- Links to articles and content related to this article
- Copyright permission to reproduce figures and/or text from this article

View the Full Text HTML

J|A|C|S
ARTICLES
Published on Web 06/03/2005

Coordination-Based Gold Nanoparticle Layers

Meni Wanunu,† Ronit Popovitz-Biro,† Hagai Cohen,‡ Alexander Vaskevich,† and Israel Rubinstein*,†

Contribution from the Departments of Materials and Interfaces and Chemical Research Support, Weizmann Institute of Science, Rehovot 76100, Israel

Received January 3, 2005; E-mail: israel.rubinstein@weizmann.ac.il

Abstract: Gold nanoparticle (NP) mono- and multilayers were constructed on gold surfaces using coordination chemistry. Hydrophilic Au NPs (6.4 nm average core diameter), capped with a monolayer of 6-mercaptohexanol, were modified by partial substitution of bishydroxamic acid disulfide ligand molecules into their capping layer. A monolayer of the ligand-modified Au NPs was assembled via coordination with Zr^{4+} ions onto a semitransparent Au substrate (15 nm Au, evaporated on silanized glass and annealed) precoated with a self-assembled monolayer of the bishydroxamate disulfide ligand. Layer-by-layer construction of NP multilayers was achieved by alternate binding of Zr^{4+} ions and ligand-modified NPs onto the first NP layer. Characterization by atomic force microscopy (AFM), ellipsometry, wettability, transmission UV−vis spectroscopy, and cross-sectional transmission electron microscopy showed regular growth of NP layers, with a similar NP density in successive layers and gradually increased roughness. The use of coordination chemistry enables convenient step-by-step assembly of different ligand-possessing components to obtain elaborate structures. This is demonstrated by introducing nanometer-scale vertical spacing between a NP layer and the gold surface, using a coordination-based organic multilayer. Electrical characterization of the NP films was carried out using conductive AFM, emphasizing the barrier properties of the organic spacer multilayer. The results exhibit the potential of coordination self-assembly in achieving highly controlled composite nanostructures comprising molecules, NPs, and other ligand-derivatized components.

Introduction

Metal nanoparticle (NP) films have been the subject of much research, primarily due to the interest in their optical and electronic properties.[1] Although actual applications of such films have yet to be realized, NP films show promise for the development of novel electrical and optical sensors, as precursors for metallic films, and as catalysts. Gold NPs are most frequently used, due to their chemical stability and relatively simple preparation. In addition, the reactivity of sulfur-containing molecules (thiols, disulfides, etc.) toward Au surfaces, enabling formation of a large variety of self-assembled monolayers (SAMs),[2] can be exploited for chemical manipulation of Au surfaces.[3]

Various techniques have been developed in recent years for the construction of metal NP films on surfaces. Strategies for immobilization of Au NP layers onto surfaces include physical deposition (e.g., spin-coating[4,5] and spraying[6]) or layer-by-layer (LbL) schemes. LbL preparation has the advantage of better control over the film thickness and density. LbL approaches that have been demonstrated include covalent schemes, primarily surface attachment of NPs via dithiol linkages[7−9] or mercaptosilanes.[10] Electrostatic binding was also shown, ranging from the use of charged molecules for attaching NPs to the surface,[11−13] to polyelectrolyte systems,[11,14−17] the latter applied also to LbL construction of NP multilayers.

There is substantial interest in the design of Au NP films with control over the spacing between NPs, particularly in the range smaller than the NP diameter,[18] where the optical and electronic properties change substantially with spacing. Control

† Department of Materials and Interfaces.
‡ Department of Chemical Research Support.

(1) Feldheim, D. L.; Foss, C. A. J. *Metal Nanoparticles*; Marcel Dekker: New York, 2002.
(2) Nuzzo, R. G.; Allara, D. L. *J. Am. Chem. Soc.* **1983**, *105*, 4481−4483.
(3) Ulman, A. *An Introduction to Ultrathin Organic Films*; Academic Press: Boston, 1991.
(4) Liu, F. K.; Chang, Y. C.; Ko, F. H.; Chu, T. C.; Dai, B. T. *Microelectron. Eng.* **2003**, *67*−*8*, 702−709.
(5) Fan, H. Y.; Yang, K.; Boye, D. M.; Sigmon, T.; Malloy, K. J.; Xu, H. F.; Lopez, G. P.; Brinker, C. J. *Science* **2004**, *304*, 567−571.
(6) Rowe, M. P.; Plass, K. E.; Kim, K.; Kurdak, C.; Zellers, E. T.; Matzger, A. J. *Chem. Mater.* **2004**, *16*, 3513−3517.
(7) Brust, M.; Bethell, D.; Schiffrin, D. J.; Kiely, C. J. *Adv. Mater.* **1995**, *7*, 795−797.
(8) Brust, M.; Etchenique, R.; Calvo, E. J.; Gordillo, G. J. *Chem. Commun.* **1996**, 1949−1950.
(9) Fishelson, N.; Shkrob, I.; Lev, O.; Gun, J.; Modestov, A. D. *Langmuir* **2001**, *17*, 403−412.
(10) Tseng, J. Y.; Lin, M. H.; Chau, L. K. *Colloids Surf., A* **2001**, *182*, 239−245.
(11) Freeman, R. G.; et al. *Science* **1995**, *267*, 1629−1632.
(12) Grabar, K. C.; Freeman, R. G.; Hommer, M. B.; Natan, M. J. *Anal. Chem.* **1995**, *67*, 735−743.
(13) Shipway, A. N.; Lahav, M.; Willner, I. *Adv. Mater.* **2000**, *12*, 993−998.
(14) Iler, R. K. *J. Colloid Interface Sci.* **1966**, *21*, 569−594.
(15) Feldheim, D. L.; Grabar, K. C.; Natan, M. J.; Mallouk, T. E. *J. Am. Chem. Soc.* **1996**, *118*, 7640−7641.
(16) Schmitt, J.; Decher, G.; Dressick, W. J.; Brandow, S. L.; Geer, R. E.; Shashidhar, R.; Calvert, J. M. *Adv. Mater.* **1997**, *9*, 61−65.
(17) Yu, A. M.; Liang, Z. J.; Cho, J. H.; Caruso, F. *Nano Lett.* **2003**, *3*, 1203−1207.
(18) Toohey, M. J. *Sens. Actuators, B* **2005**, *105*, 232−250.

over interparticle spacing in Au NP films was demonstrated using Au@SiO_2 core−shell NPs with varying thickness of the insulating SiO_2 shell.[19] Controlled spacing of NP layers, either from the substrate or between layers, can be achieved by using α,ω-alkanedithiols, but this approach is of limited use due to the unavailability of alkanedithiols > 2 nm in length.[20]

Coordination chemistry offers simplicity, stable bonding, and ligand−metal specificity, enabling ligand-bearing components to be assembled into supramolecular structures using appropriate metal ions.[21−23] This approach is particularly compatible with surface chemistry, as binding of metal ions activates the surface toward ligand binding, and vice versa.[24−28] The use of different building blocks containing similar ligand functionalities provides a universal, LEGO-type binding scheme, where the same chemistry is used for binding different components into a composite nanostructure. This strategy is attractive for LbL schemes, adding one coordinated layer in each step. Murray and co-workers investigated coordinated NP films prepared by repetitive adsorption of carboxylate-modified Au NPs and divalent metal ions (Cu^{2+}, Zn^{2+}, Pb^{2+}).[29−33] In these systems, several NP monolayers are deposited in each dip cycle, while the interparticle spacing was shown to be lower than expected for coordinative carboxylate−metal ion binding. Chen and co-workers obtained similar results with pyridine-functionalized Au NPs and Cu^{2+} ions, studied by quartz crystal microbalance measurements.[34] These observations suggest that Cu^{2+}-based coordination systems induce insertion of excess ions to the periphery of the NPs, resulting in poorly controlled growth.

In the present work, hydroxyl-functionalized, hydrophilic Au NPs were prepared and derivatized with a disulfide bishydroxamate ligand by partial replacement of the hydroxyl capping layer with ligand molecules. The ligand-bearing NPs were used for the construction of layered NP architectures on surfaces by coordination with Zr^{4+} ions, depositing one NP layer in each step in a true LbL fashion. Monolayers and multilayers of Au NPs on semitransparent Au substrates were prepared and characterized by atomic force microscopy (AFM), ellipsometry, UV−vis spectroscopy, water contact angles, and cross-sectional transmission electron microscopy (TEM). Controlled spacing of NP layers from the surface was demonstrated by binding the Au NPs onto a 4.5-nm-thick organic multilayer, where the NPs and spacer layer are assembled using the same coordination chemistry. The latter demonstrates not only the possibility to obtain spaced NP layers in a highly controlled way, but also the convenience of coordination self-assembly in the construction of composite nanostructures including molecular and NP components.

Experimental Section

Chemicals and Materials. The synthesis of the bishydroxamate disulfide ligand **1** (Figure 1a) was described previously.[35] The synthesis of the branched hexahydroxamate ligand **2** (Figure 1c) is given elsewhere.[36] 6-Mercaptohexanol (MH) (97%, Aldrich) was vacuum distilled prior to use. All other solvents and chemicals were analytical grade and used as received. Water was triply distilled. Samples were dried using filtered household N_2 (>99%).

Gold Substrates. The semi-transparent Au substrates were prepared by evaporation of 15-nm Au on glass substrates pretreated with 3-aminopropyl trimethoxysilane, followed by postdeposition annealing in air (200 °C, 20 h). More details on the Au substrates are given elsewhere.[37]

Synthesis of Mercaptohexanol-Capped Au NPs. Au NPs were synthesized in toluene using tetraoctylammonium bromide (TOAB) as the stabilizer,[7,38] followed by exchange of the TOAB stabilizer with 6-mercaptohexanol, as shown schematically in Figure 1a. The detailed preparation procedure was as follows: Into a stirred solution of TOAB (600 mg, 1.09 mmol) in 40 mL of toluene, a solution of $HAuCl_4$ (200 mg, 0.52 mmol) in 20 mL of H_2O was added. After 5 min, the biphasic solution was separated and the organic phase (deep orange color) was placed in a 100-mL flask and stirred vigorously. A solution of $NaBH_4$ (200 mg, 5.25 mmol) in 15 mL of H_2O was added dropwise over a period of 10 min, during which the color of the solution changed to ruby red. After the solution was stirred for 1−1.5 h, the two phases were separated and the organic phase was vigorously washed with 0.1 M HCl (15 mL), 0.1 M NaOH (15 mL), H_2O (3 × 15 mL), and saturated brine (20 mL). The resulting toluene solution of TOAB-capped NPs was stored in a glass bottle under N_2 atmosphere.

Exchange of the TOAB capping layer with MH was performed as follows: To a stirred solution of MH (100 μL, 0.73 mmol) in 10 mL of DMF, a solution of TOAB-capped Au NPs in toluene (20 mL) was added dropwise under N_2 atmosphere. No significant color change was observed during the addition, indicating that the NPs remained stable. The solution was stirred for 2 h, after which the solvents were concentrated to 0.5 mL, and *i*-PrOH was added (ca. 10 mL) and evaporated to near dryness (∼0.2 mL). Addition of *i*-PrOH (0.5 mL) followed by acetone (30 mL) resulted in flocculation of the NPs, indicated by the gradual formation of a purple suspension. Centrifugation of the suspension and removal of the solvent, followed by addition of *i*-PrOH (0.5 mL) and acetone (30 mL), precipitated the NPs. This process was repeated four times to ensure removal of excess MH and TOAB. The NP precipitate was then dried in a 15-mL polypropylene Falcon tube by treatment with N_2 and overnight vacuum. The NPs were found to be stable in a vacuum for long time periods (weeks), dissolving upon addition of DMF to give a ruby-red solution.[39] The resulting MH-

(19) Ung, T.; Liz-Marzan, L. M.; Mulvaney, P. *J. Phys. Chem. B* **2001**, *105*, 3441−3452.
(20) Brust, M.; Bethell, D.; Kiely, C. J.; Schiffrin, D. J. *Langmuir* **1998**, *14*, 5425−5429.
(21) Semenov, A.; Spatz, J. P.; Moller, M.; Lehn, J. M.; Sell, B.; Schubert, D.; Weidl, C. H.; Schubert, U. S. *Angew. Chem., Int. Ed.* **1999**, *38*, 2547−2550.
(22) Tominaga, M.; Suzuki, K.; Kawano, M.; Kusukawa, T.; Ozeki, T.; Sakamoto, S.; Yamaguchi, K.; Fujita, M. *Angew. Chem., Int. Ed.* **2004**, *43*, 5621−5625.
(23) Yamaguchi, T.; Tashiro, S.; Tominaga, M.; Kawano, M.; Ozeki, T.; Fujita, M. *J. Am. Chem. Soc.* **2004**, *126*, 10818−10819.
(24) Hatzor, A.; van der Boom-Moav, T.; Yochelis, S.; Vaskevich, A.; Shanzer, A.; Rubinstein, I. *Langmuir* **2000**, *16*, 4420−4423.
(25) Hatzor, A.; Moav, T.; Cohen, H.; Matlis, S.; Libman, J.; Vaskevich, A.; Shanzer, A.; Rubinstein, I. *J. Am. Chem. Soc.* **1998**, *120*, 13469−13477.
(26) Ansell, M. A.; Cogan, E. B.; Neff, G. A.; von Roeschlaub, R.; Page, C. J. *Supramol. Sci.* **1997**, *4*, 21−26.
(27) Evans, S. D.; Ulman, A.; Goppertberarducci, K. E.; Gerenser, L. J. *J. Am. Chem. Soc.* **1991**, *113*, 5866−5868.
(28) Lee, H.; Kepley, L. J.; Hong, H. G.; Mallouk, T. E. *J. Am. Chem. Soc.* **1988**, *110*, 618−620.
(29) Hicks, J. F.; Zamborini, F. P.; Murray, R. W. *J. Phys. Chem. B* **2002**, *106*, 7751−7757.
(30) Zamborini, F. P.; Leopold, M. C.; Hicks, J. F.; Kulesza, P. J.; Malik, M. A.; Murray, R. W. *J. Am. Chem. Soc.* **2002**, *124*, 8958−8964.
(31) Templeton, A. C.; Zamborini, F. P.; Wuelfing, W. P.; Murray, R. W. *Langmuir* **2000**, *16*, 6682−6688.
(32) Zamborini, F. P.; Smart, L. E.; Leopold, M. C.; Murray, R. W. *Anal. Chim. Acta* **2003**, *496*, 3−16.
(33) Zamborini, F. P.; Hicks, J. F.; Murray, R. W. *J. Am. Chem. Soc.* **2000**, *122*, 4514−4515.
(34) Chen, S. W.; Pei, R. J.; Zhao, T. F.; Dyer, D. J. *J. Phys. Chem. B* **2002**, *106*, 1903−1908.
(35) Moav, T.; Hatzor, A.; Cohen, H.; Libman, J.; Rubinstein, I.; Shanzer, A. *Chem.−Eur. J.* **1998**, *4*, 502−507.
(36) Wanunu, M.; Vaskevich, A.; Arad-Yellin, R.; Shanzer, A.; Rubinstein, I. In preparation.
(37) Wanunu, M.; Vaskevich, A.; Rubinstein, I. *J. Am. Chem. Soc.* **2004**, *126*, 5569−5576.
(38) Gittins, D. I.; Caruso, F. *Chemphyschem* **2002**, *3*, 110−113.
(39) Several hours were required to completely dissolve the NP precipitate in DMF due to the formation of highly stable solids during the vacuum treatment.

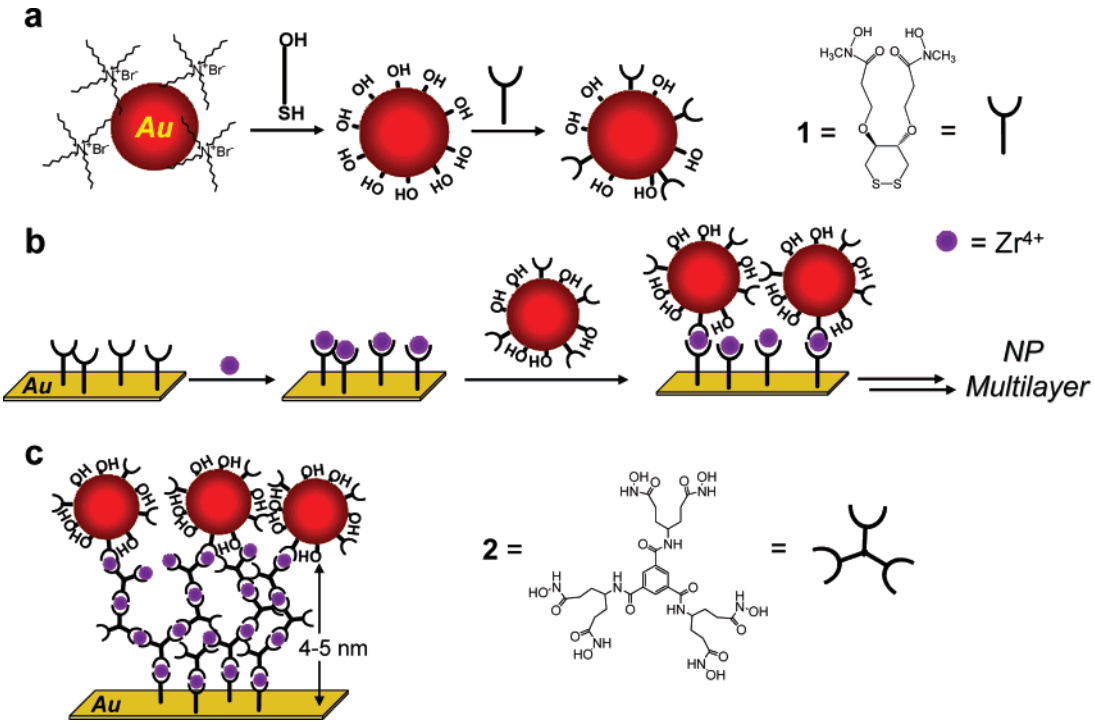

Figure 1. Schematic presentations of: (a) Preparation of ligand-functionalized Au NPs from TOAB-capped NPs; also shown is the chemical structure of ligand **1**. (b) Stepwise assembly of ligand-bearing Au NP multilayers on ligand-functionalized Au surfaces. (c) Spacing of a NP monolayer from the Au surface using a Zr^{4+}-coordinated organic multilayer of **2**; the chemical structure of **2** is shown.

capped NP solution (quantitative yield) was stored at −15 °C. The exchange of TOAB with MH was verified by ^{1}H NMR spectroscopy (in deuterated DMF), showing peaks for MH but not for TOAB.

Place-Exchange of MH-Capped Au NPs with Bishydroxamate Disulfide 1. The reaction is shown schematically in Figure 1a. Into a stirred solution of MH-capped NPs (20 mg) in DMF (5 mL), a solution of **1** (3 mg) in DMF (1 mL) was added. The solution was stirred for 1 week to ensure incorporation of **1** into the NP capping layer. The NPs were then cleaned by evaporation of the solvent to near dryness and addition of *i*-PrOH, followed by precipitation from acetone, in an analogous fashion to cleaning of the MH-capped NPs. The NPs were then dissolved in 30% aq. DMF and centrifuged (~7000 rpm, 5 min) to remove small amounts of precipitates. The resultant NPs (ca. 50% yield) are denoted [MH + **1**]-capped Au NPs.

Self-Assembly of [MH + 1]-Capped Au NP Layers. A self-assembled monolayer (SAM) of **1** was prepared by dipping a cleaned Au substrate[40] into a 3 mM solution of **1** in 1:1 EtOH:$CHCl_3$ overnight, followed by washing in $CHCl_3$ and EtOH. Zr^{4+} binding was carried out by immersion in a 1 mM ethanolic solution of $Zr(acac)_4$ for 1 h, followed by washing in EtOH. Immersion in a solution of [MH + **1**]-capped Au NPs (~0.1 μM) in 30% aq. DMF overnight, followed by rinsing and sonication[41] with 30% aq. DMF (5 min), afforded a coordinated NP monolayer. Alternate binding of Zr^{4+} and [MH + **1**]-capped NPs resulted in coordinated NP multilayers, as shown schematically in Figure 1b.

Spacing of a NP Layer from the Gold Surface. Onto a SAM of **1** coordinated with Zr^{4+} ions, a monolayer of the branched ligand molecule **2** was assembled by dipping into a 1 mM solution of **2** in MeOH for 3 h, followed by washing in MeOH. Three layers of **2**/Zr^{4+} were similarly assembled in a step-by-step manner, followed by binding of [MH + **1**]-capped NPs (Figure 1c).

AFM. Dynamic-mode AFM measurements were carried out in ambient air, using a PicoSPM instrument (Molecular Imaging, USA). The tips used in all dynamic mode measurements were NSC12 (MikroMasch, Estonia) at a resonant frequency of ca. 100 kHz. Since the AFM tip shape strongly affects the apparent topography, deconvolution of the images[42] was performed to verify that the tips have a radius of ca. 10 nm. AFM profilometry was performed in the contact mode by abrasion of a section of the film using contact-mode AFM tips CSC12 (MikroMasch) followed by measurement of the line profile using the same tip in the dynamic mode. The average height of 10−15 line scans is reported. Conductive AFM measurements were carried out at 296 ± 1 K and 40 ± 10% relative humidity, using a Pt-coated Si tip (NSC14/Pt, MikroMasch, Estonia) at a feedback contact force of 1−3 nN. The tip was grounded, and the sample bias was controlled using the scanning tunneling microscopy circuitry of the PicoSPM. The same tip was used in all experiments, and the experiments were repeated in reverse order to rule out tip degradation artifacts.

Cross-Sectional TEM of NP Films. The NP films showed incompatibility with the commonly used thiol-based resins and were therefore embedded in a phenol-based M-Bond 610 epoxy resin (Ted Pella Inc., USA). A 4 × 8 mm^2 block of epoxy was prepared by casting the resin solution into a rubber mold (Structure Probe Inc., USA) and curing for 3 days at 60 °C. The block was glued onto the film by placing 2 drops of the resin between the epoxy block and the film, followed by curing. The glass backing was then removed by breaking it off the gold (the glass was first chipped to facilitate its removal), and ca. 200 μL of resin solution was placed on the backside of the gold, followed by curing. The embedded samples were then sectioned into thin (35−50 nm) slices using a diamond knife (Micro Star 45°) and a Leica ULTRACUT UCT Ultramicrotome. The samples were sliced perpendicular to the surface of the sample and placed on carbon/collodion-coated copper grids. TEM imaging was performed with a Philips CM-120 transmission electron microscope operating at 120 kV, equipped with a charge-coupled device camera (2kx2k Gatan Ultrascan 1000).

Ellipsometry. Ellipsometric measurements were carried out with a Rudolph Research Auto-EL IV null ellipsometer, at an angle of

(40) Ron, H.; Matlis, S.; Rubinstein, I. *Langmuir* **1998**, *14*, 1116−1121.
(41) We found sonication to be crucial for removing excessive amounts of physisorbed NPs from the surface, as indicated by AFM and UV−vis spectroscopy.
(42) Tip shape analysis was performed using a free version of SPIP software, Image Metrology A/S, Denmark (http://www.imagemet.com).

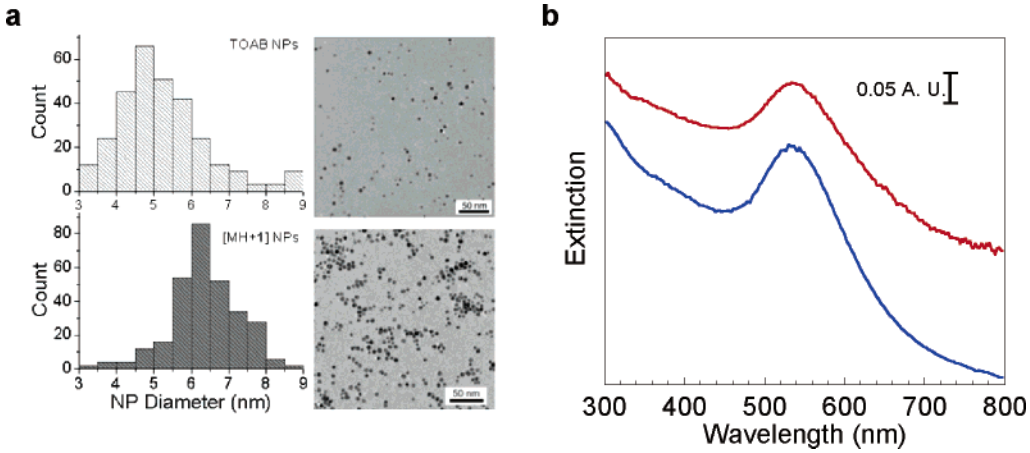

Figure 2. (a) TEM images and size-distribution histograms of TOAB-capped and [MH + **1**]-capped Au NPs. (b) Solution UV−vis spectra of TOAB-capped NPs in toluene (top) and [MH + **1**]-capped NPs in DMF (bottom).

incidence $\phi = 70°$ and a wavelength $\lambda = 632.8$ nm. The same four points were measured on each sample before and after self-assembly. Simulated $\Delta-\Psi$ curves were generated using a literature procedure.[43] Since the substrate was a semitransparent Au film on glass, a three-layer model was used, i.e., glass/Au/film. The substrate was modeled as glass ($n = 1.52$, $k = 0$)/gold ($n = 0.197$, $k = 3.45$ at $\lambda = 632.8$ nm)[44] using a gold film thickness of 18 nm (from ellipsometry). Fitting of the effective Au film thickness takes into account changes in the interfaces upon annealing of the substrates.[9] The dielectric function of the NP film was assumed to be constant during multilayer growth.

Contact-Angle (CA) Measurements. Advancing water CAs were measured using a computerized CA meter (KSV Instruments, Finland). Data collection and analysis were carried out using the provided CAM100 software. CAs were measured on three different spots in each sample.

Transmission UV−Vis Spectroscopy. Transmission spectra were obtained with a Varian Cary 50 UV−vis spectrophotometer. All measurements were carried out in air, using a homemade holder designed for reproducibility of the sampled spot. Spectra were recorded using air as baseline.

X-ray Photoelectron Spectroscopy (XPS). XPS measurements were carried out with a Kratos Axis HS XPS system, using a monochromatized Al (Kα) X-ray source ($h\upsilon = 1486.6$ eV). To minimize beam-induced damage, a low dose was maintained, using a relatively low beam flux (5 mA emission current at 15 keV). Pass energies of 20−80 eV were used.

Results and Discussion

Gold NPs. Figure 2a shows TEM images and size-distribution histograms for TOAB-capped and [MH + **1**]-capped Au NPs. The images show that the NPs are approximately spherical, with an average Au core diameter of 5.2 ± 1.2 nm for TOAB-capped NPs, whereas after exchange with MH + **1**, the average NP core diameter is 6.4 ± 0.9 nm. The increase in average diameter is explained by enrichment of larger NPs during the precipitation steps following exchange of **1** into the capping layer. The precipitation, resulting in a certain loss of NPs, narrows significantly the NP size distribution by eliminating smaller NPs, as shown in Figure 2a. UV−vis spectra of the NP solutions are shown in Figure 2b. A 6-nm red shift in λ_{max} is observed following NP stabilizer partial exchange, attributed to the change of solvent, capping layer, and Au core size. The [MH + **1**]-capped NPs were dissolved in a DMF:H_2O mixture, for which a pH of 8.6 was measured. Acidification of this sol (0.1 M HCl) to pH < 5.0 resulted in flocculation of the NPs, observed as a significant red shift in the spectrum, followed by a nearly irreversible precipitation. Otherwise, the sol is stable for months.

The fraction of **1** in the NP capping layers was estimated by measuring the N:S atomic ratio in XPS measurements of a coordinated multilayer film of [MH + **1**]-capped NPs on Au substrate. The chemical formulas of **1** and MH are $C_{12}H_{22}O_6N_2S_2$ and $C_6H_{14}OS$, respectively. The composition of the capping monolayer on the [MH + **1**]-capped NPs was estimated using the relative atomic concentrations of N and S. Several XPS experiments performed at two different takeoff angles (90° and 30°) gave a N:S ratio corresponding to 14 ± 4% exchange of **1** on the NP surface. Attempts to verify the degree of exchange using ^{1}H NMR spectroscopy in deuterated DMF were unsuccessful due to solvent interference and insufficient signal by the small fraction of **1** in the capping layer. The partially ligand-substituted capping layer on the NPs maintains the hydrophilic nature of the NPs while providing the coordination capabilities of the ligand, as shown below.

Au NP Monolayers. Assembly of coordinated Au NP monolayers is shown schematically in Figure 1b. The self-assembly scheme is similar to those applied previously by us,[25,45] using Zr^{4+} ions for coordination between ligand (bishydroxamate) bearing components. A SAM of **1** was prepared on the Au substrate, followed by Zr^{4+} binding from $Zr(acac)_4$ solution.[45] A monolayer of [MH + **1**]-capped NPs was then assembled by coordination to the bound Zr^{4+} ions.

Figure 3 shows dynamic-mode AFM images of a bare Au substrate and a coordinated NP monolayer on the Au surface. The root-mean-square (RMS) roughness in the bare Au image is 1.0 nm, whereas that in the NP monolayer image is 2.2 nm. The brighter spots arise from maximization of the contrast in the AFM images, which was purposely done to optimize the image quality. Individual NPs can be seen throughout the NP monolayer image, with a minimum lateral spacing of ca. 8.5 nm between NP centers; the latter can be compared with the average NP diameter, 8.1 nm (6.4 nm core diameter + 1.7 nm for two organic ligands). The image shows a single layer of

(43) Azzam, R. M. A.; Bashara, N. M. *Ellipsometry and Polarized Light*; North-Holland: Amsterdam, 1977.
(44) Innes, R. A.; Sambles, J. R. *J. Phys. F* **1987**, *17*, 277−287.
(45) Doron-Mor, I.; Cohen, H.; Cohen, S. R.; Popovitz-Biro, R.; Shanzer, A.; Vaskevich, A.; Rubinstein, I. *Langmuir* **2004**, *20*, 10727−10733.

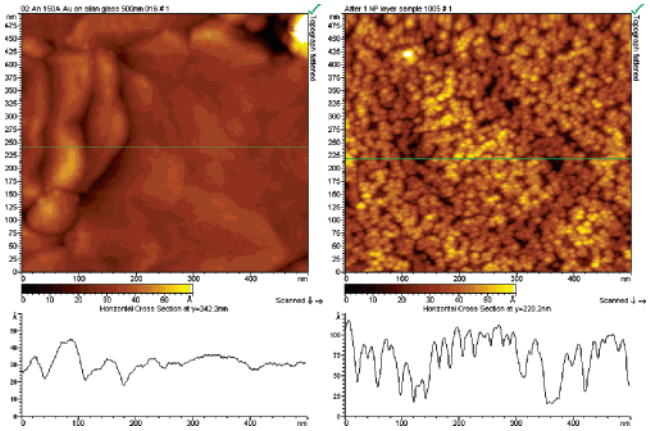

Figure 3. AFM images (500 × 500 nm^2) and *z* profiles of a bare Au surface (Left) and a similar surface covered with a monolayer of [MH + **1**]-capped Au NPs (right).

NPs, with some height fluctuations. The NP layer thickness, measured at voids in the layer, is 6−9 nm, in agreement with the NP size distribution (Figure 2a). The real coverage of the NP monolayer was calculated by counting the number of NPs in 100 × 100 nm^2 sections of the images and dividing by the theoretical number of NPs in an ideal hexagonally packed monolayer of NPs in the same area. The coverage thus calculated is ca. 54%, corresponding to a number density of 90 NPs/100 × 100 nm^2. Such a NP monolayer coverage is considerably larger than that obtained in systems where electrostatic assembly is applied,[17,46−48] for which the coverage is usually <30% due to interparticle Coulombic repulsion. Thus, the uncharged character of the [MH + **1**]-capped NPs may be responsible for the high coverage observed. The NP density obtained from AFM was homogeneous in different areas of the sample, displaying <5% regional variability. The extinction of a NP monolayer film, averaged for numerous films, was 0.03 ± 0.01 au (see Figure 4), measured at the wavelength of maximum plasmon absorbance; the latter was always in the range 535−540 nm. A control experiment in which a SAM of **1** (without Zr^{4+}) was exposed to [MH + **1**]-capped NPs resulted in no binding of NPs (measured spectroscopically, see Supporting Information), establishing the role of Zr^{4+} coordination in the NP binding.

Au NP Multilayers. LbL construction of coordination NP multilayers is shown schematically in Figure 1b. A SAM of **1** was prepared on the Au substrate, followed by sequential binding of Zr^{4+} and [MH + **1**]-capped NPs, to form a NP monolayer as detailed above. This was followed by alternate binding of Zr^{4+} and [MH + **1**]-capped NPs, yielding coordinated NP multilayers.

Figure 4 shows transmission UV−vis spectra obtained during the construction of a NP multilayer on the semitransparent Au substrate. The absolute spectra (Figure 4a) show the characteristic extinction of the semitransparent Au film, followed by a gradual increase of the extinction in the region 300−650 nm accompanying LbL accumulation of NP layers. A concomitant decrease in the extinction is observed at wavelengths longer than ca. 650 nm; a similar effect was previously reported for semitransparent Au films covered with mono- and multilayers

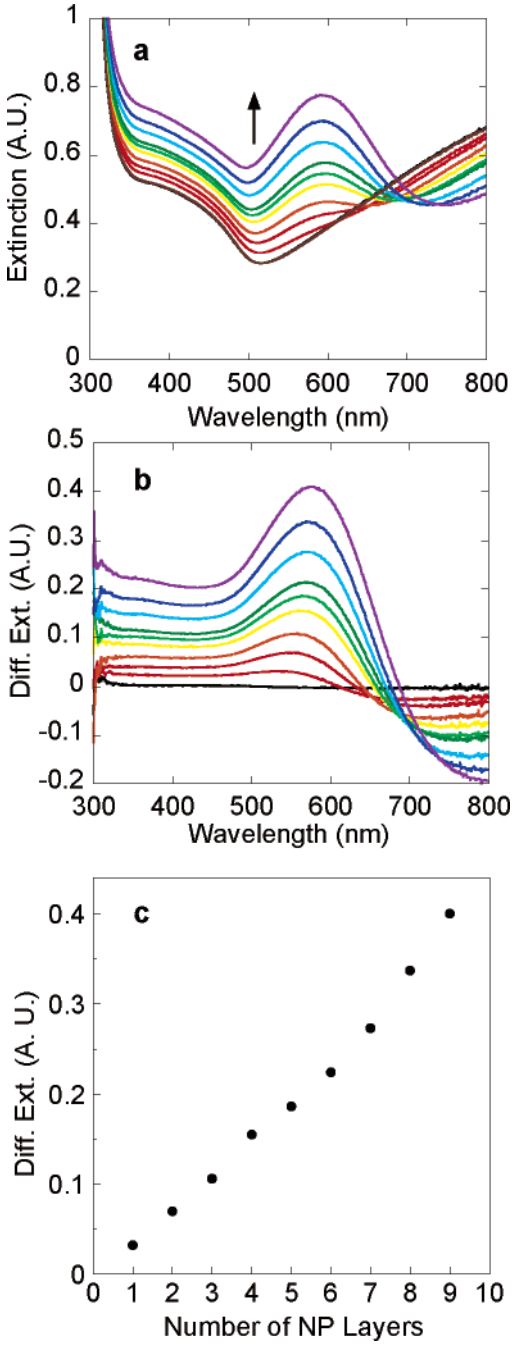

Figure 4. (a) Absolute transmission UV−vis spectra obtained during coordination self-assembly of a multilayer of [MH + **1**]-capped Au NPs on a semitransparent Au substrate; the lowest curve is the spectrum of the Au substrate coated with a monolayer of **1** coordinated with Zr^{4+} ions. (b) Difference spectra obtained by subtracting the spectrum of a bare Au substrate from the spectra in a. (c) Plot of the maximum differential extinction vs number of NP layers (data from b).

of Au NPs.[49,50] The optical changes that cause this phenomenon are yet unresolved, i.e., a decrease in the absorbance and/or reflectivity of the coated Au surface. Difference spectra obtained by subtracting the Au substrate extinction (Figure 4b) show the characteristic Au NP surface plasmon resonance band, gradually increasing as more NP layers are added, with a small red shift of the extinction maximum. A regular change in the extinction

(46) Grabar, K. C.; et al. *Langmuir* **1996**, *12*, 2353−2361.
(47) Schmitt, J.; Machtle, P.; Eck, D.; Mohwald, H.; Helm, C. A. *Langmuir* **1999**, *15*, 3256−3266.
(48) Baum, T.; Bethell, D.; Brust, M.; Schiffrin, D. J. *Langmuir* **1999**, *15*, 866−871.
(49) Kuther, J.; Seshadri, R.; Nelles, G.; Butt, H. J.; Knoll, W.; Tremel, W. *Adv. Mater.* **1998**, *10*, 401−404.
(50) Okamoto, T.; Yamaguchi, I. *J. Phys. Chem. B* **2003**, *107*, 10321−10324.

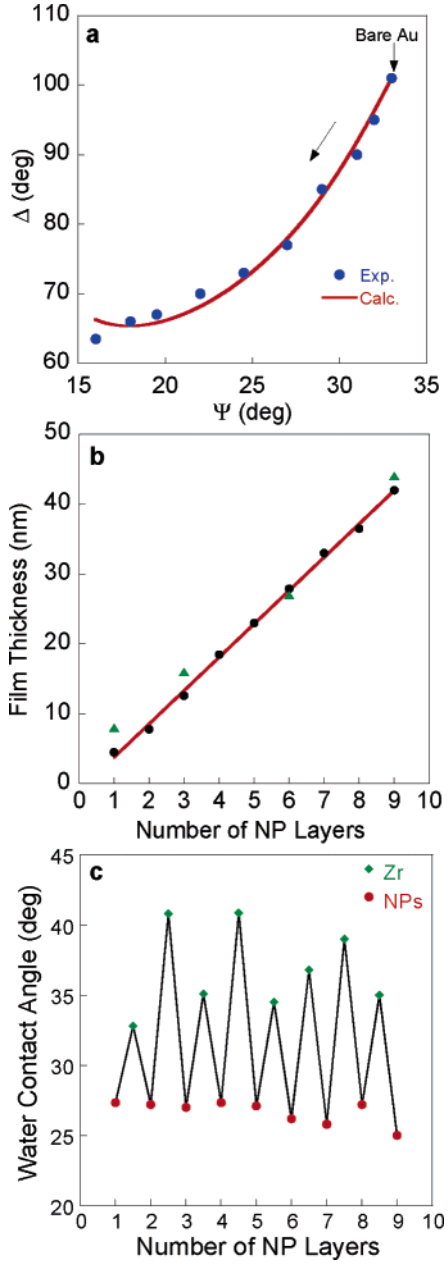

Figure 5. (a) Experimental Δ and Ψ values (points) obtained during NP multilayer construction and calculated Δ−Ψ trajectory (solid line) obtained using $n_f = 2.43$, $k_f = 1.33$. (b) Ellipsometric (circles) and TEM cross-section (triangles) film thickness values as a function of the number of NP layers. (c) Advancing water contact angles measured during the construction of the NP multilayer.

with a nearly constant increment is observed in the 300−600-nm region. A plot of the maximum differential extinction for NP multilayer construction (Figure 4c) shows a nearly linear increase of the extinction upon binding of NP layers. The extinction increase at λ_{max}, given by the slope of the curve in Figure 4c, is 0.025−0.03 au per NP layer, similar to the extinction of the first NP monolayer (see above). The positive deviation from linearity observed at higher layer numbers may be due to an increase in the roughness of the films, hence, binding of more NPs per layer.

Changes in the ellipsometric parameters Δ and Ψ during sequential assembly of NP multilayers are shown in Figure 5a. The data were fitted by assuming a constant dielectric function for the NP film. Theoretical Δ−Ψ trajectories were simulated for films with different n_f and k_f values in order to minimize the deviation from the experimental Δ−Ψ values. The best-fit Δ−Ψ trajectory, shown as the solid line in Figure 5a, was obtained using $n_f = 2.43$, $k_f = 1.33$ ($\lambda = 632.8$ nm, $\phi = 70°$). Thicknesses were calculated by determining the points on the simulated trajectory closest to the experimental data points. The optical constants n_f and k_f obtained are in agreement with those reported for NP films with dithiol spacers.[20,48,51] On the other hand, substantially different optical constants, more reminiscent of bulk Au, were reported for NP multilayer stabilized with ω-mercaptoundecanoic acid, indicating aggregation of the NPs on the surface.[52] These reports demonstrate the critical role of interparticle distance in Au NP films on the dielectric properties of the films.[51] The present ellipsometric results on the coordinated NP multilayer films suggest that the expected distance between adjacent NPs, 1.7 nm (the length of two molecules of **1** coordinated with Zr^{4+} ion), is maintained in the assembly. The latter is consistent with the spectroscopic data (Figure 4), where the general shape of the NP surface plasmon band is maintained with only a minor red shift in the extinction maximum with added layers.

Figure 5b shows the ellipsometric NP film thickness, calculated as detailed above, vs the number of NP layers. Growth of the NP multilayer (up to 9 layers) is highly regular, with a constant increase of 4.8 nm/NP monolayer, in good agreement with the TEM imaging results shown below.

Figure 5c shows advancing water CAs measured during Au NP multilayer construction. The hydrophilic behavior of the NPs in solution (i.e., their solubility in DMF:H_2O) is reflected in the low CAs on the NP-terminated surfaces (25−30°), while the Zr^{4+}-terminated surfaces are more hydrophobic due to partial acac termination. The oscillatory wetting behavior is consistent with similar coordination multilayer systems,[25,36,45] indicating again regular growth of the NP multilayer.

Parts a−d of Figure 6 show a series of AFM images of 1, 3, 6, and 9 NP layers on the Au substrate. The density of the NPs is high in all layers, with an increase in the RMS roughness of successive layers. The experimental RMS roughness in parts a−d of Figure 6 is 2.2, 2.7, 3.1, and 3.5 nm, respectively. The AFM images and roughness values are consistent with regular growth of NP layers with a small increase in the number of NPs per added layer (see Figure 4c).

Direct visualization of the multilayered NP structure can be obtained by cross-sectional TEM imaging,[16,53−58] as shown in parts e−h of Figure 6. Such images enable direct determination of the film thickness, number of NP layers, and film morphology. The gradual increase in the number of NP layers, consistent with the number of binding steps, is evident. Two points should be considered when analyzing the cross-sectional images: (i) The width of a section is ca. 50 nm, i.e., the span of 5−6 NPs.

(51) Zhang, H. L.; Evans, S. D.; Henderson, J. R. *Adv. Mater.* **2003**, *15*, 531−534.
(52) Auer, F.; Scotti, M.; Ulman, A.; Jordan, R.; Sellergren, B.; Garno, J.; Liu, G. Y. *Langmuir* **2000**, *16*, 7554−7557.
(53) Joseph, Y.; et al. *J. Phys. Chem. B* **2003**, *107*, 7406−7413.
(54) Cho, S. H.; Lee, S.; Ku, D. Y.; Lee, T. S.; Cheong, B.; Kim, W. M.; Lee, K. S. *Thin Solid Films* **2004**, *447*, 68−73.
(55) Sun, K.; Zhu, S.; Fromknecht, R.; Linker, G.; Wang, L. M. *Mater. Lett.* **2004**, *58*, 547−550.
(56) Palmer, R. E.; Pratontep, S.; Boyen, H. G. *Nat. Mater.* **2003**, *2*, 443−448.
(57) Durr, A. C.; Schreiber, F.; Kelsch, M.; Dosch, H. *Ultramicroscopy* **2003**, *98*, 51−55.
(58) Durr, A. C.; Schreiber, F.; Kelsch, M.; Carstanjen, H. D.; Dosch, H.; Seeck, O. H. *J. Appl. Phys.* **2003**, *93*, 5201−5209.

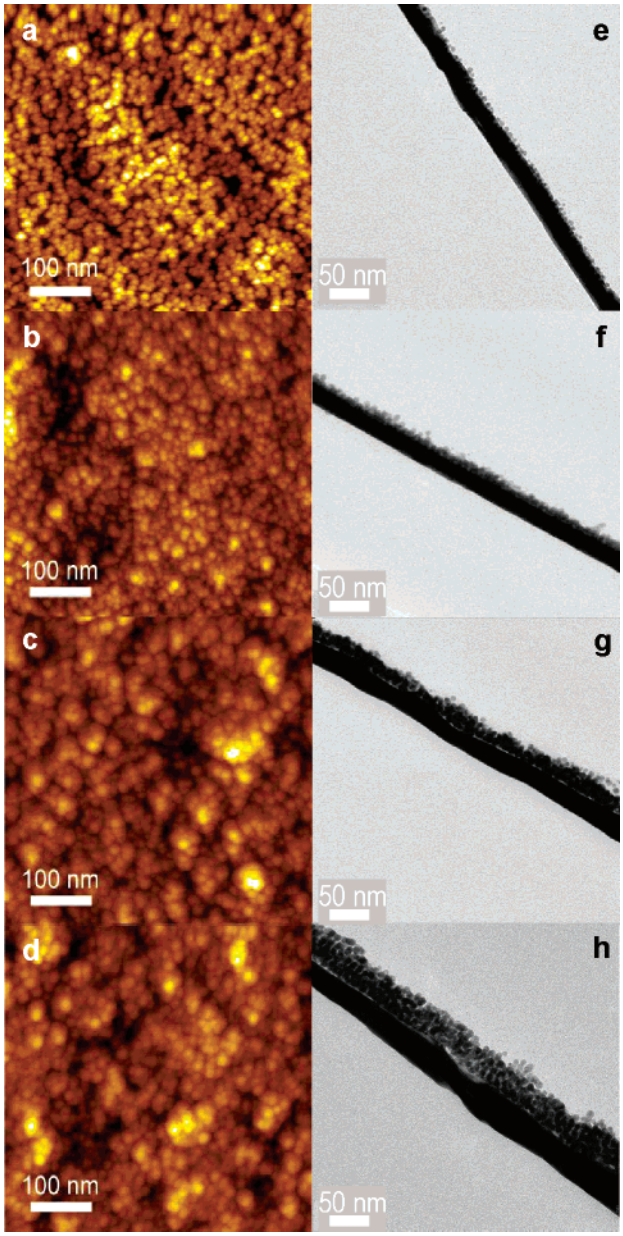

Figure 6. AFM (a−d) and cross-sectional TEM (e−h) images of 1, 3, 6, and 9 coordinated NP layers on the Au substrate.

Therefore, fluctuations in the morphology of the Au substrates give rise to higher apparent thickness in some observed regions. (ii) When the orientation of the slice is precisely normal to the substrate plane, a thin gap is seen between the substrate and the NP layer, corresponding to the first ligand monolayer; absence of this gap indicates a slightly skewed orientation.

Film thicknesses were evaluated from the cross-sectional images by measuring the distance from the Au substrate to the edge of the NP film. The average values are 8, 16, 27, and 44 nm for 1, 3, 6, and 9 layers, respectively. The thickness of a monolayer of Au NPs agrees well with the expected thickness of a monolayer film, based on a mean NP core diameter of 6.4 nm and a 1.7-nm organic ligand thickness. From the TEM images, the increase in thickness for each additional NP layer is 4.9 nm/layer, in good agreement with the ellipsometric thickness increment of 4.8 nm/layer (Figure 5b). For comparison, the theoretical value for a 3-D hexagonally packed NP lattice is 0.817 D_{NP} per layer, i.e., a 6.6-nm increment (D_{NP} is 8.1 nm,

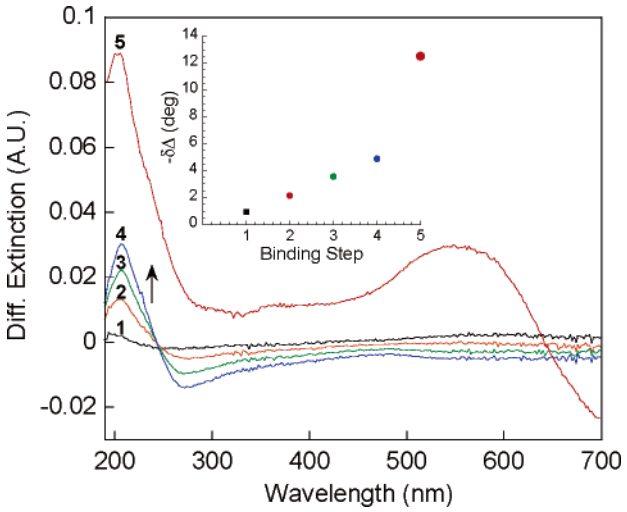

Figure 7. Transmission UV−vis difference spectra obtained during the assembly of a spaced NP monolayer, bound onto four coordinated organic layers (1 = SAM of **1**, 2−4 = layers of **2**, 5 = NP layer). Inset: Changes in the ellipsometric Δ during the assembly process.

the sum of the average core diameter and two ligand layers). The lower experimental thickness increment per layer (by ca. 26%) may be related to the packing density in the first layer (ca. 54% vs hexagonal close packing, see above), which introduces voids, enabling some interpenetration between NP layers.

The long-term stability of NP multilayer films was tested by ellipsometry and transmission UV−vis spectroscopy. Films that were stored either under ambient conditions or in dry atmosphere showed identical optical properties after 2 months.

Vertical Spacing of NP Layers. The versatility of coordination-based supramolecular architectures derives from the possibility to use a variety of ligand-bearing building blocks and a universal linking method to produce desired structures. This is demonstrated here by introducing controlled vertical spacing of a NP layer from the Au substrate. The spacer comprised a four-layer Zr^{4+}-coordinated multilayer composed of one layer of the anchor **1** followed by three layers of the branched organic ligand **2**, constructed in a LbL fashion (See Figure 1c). Details on the preparation and properties of such branched coordination multilayers are given elsewhere.[36] Similar coordination binding of NPs onto the organic multilayer followed, providing a NP layer displaced from the Au substrate by a controlled multilayer spacer.

Figure 7 shows transmission UV−vis spectra recorded during the construction of a spaced NP layer. The gradually increasing absorbance of **2** (λ_{max} = 208 nm, $\epsilon = 2.9 \times 10^4$ mol^{-1} cm^{-1}) and the appearance of the Au NP surface plasmon band after NP binding enable to follow the assembly process. The negative extinction difference centered at ~260 nm is consistent with previous reports on thin dye films on metal substrates.[59] AFM imaging (Figure 8a, compare with Figure 3b) as well as the NP absorbance of 0.03 au (Figure 7, compare with Figure 4b) indicate that the coverage of the NP monolayer on the spacer multilayer (**1** + 3 × **2**) is comparable to that of a NP monolayer assembled directly on a monolayer of the anchor **1**. The surface plasmon absorption maximum for the spaced NP layer is 552

(59) Fischer, U. C.; Bortchagovsky, E.; Heimel, J.; Hanke, R. T. *Appl. Phys. Lett.* **2002**, *80*, 3715−3717.

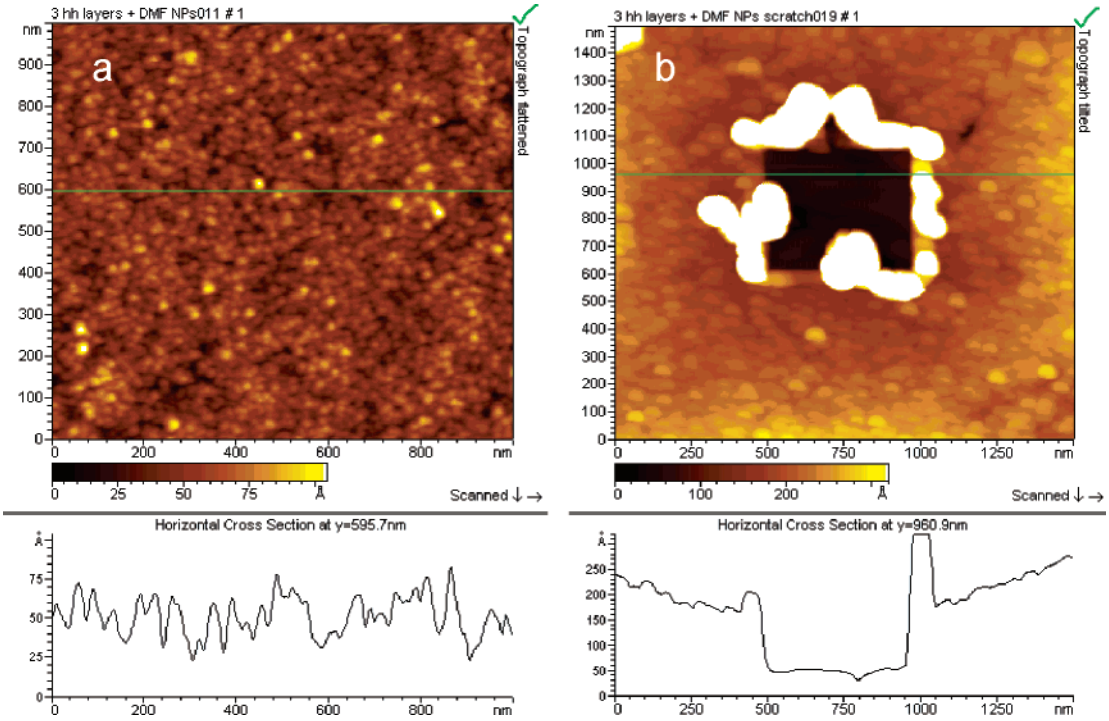

Figure 8. AC-mode AFM images and *z* profiles of (a) a NP monolayer (1000 × 1000 nm^2) assembled on a coordinated organic multilayer, as in Figure 7; (b) the same film as in (a) (1500 × 1500 nm^2) after removal of a 500 × 500 nm^2 section using the contact mode, showing the expected total film thickness of 12.5 ± 1 nm.

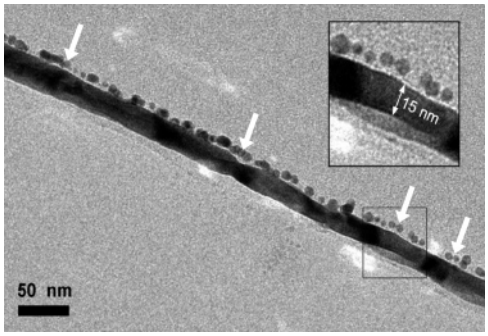

Figure 9. Cross-sectional TEM image of a NP monolayer bound on a coordinated organic multilayer, as in Figures 1c and 7. Inset: Enlarged section showing the true thickness of the evaporated gold film (15 nm), thus confirming alignment of the slice. White arrows indicate regions where a 3−4-nm spacing between the NPs and the Au substrate is observed.

nm, compared with 538 nm for the NP layer on a monolayer of **1**. The inset in Figure 7 shows ellipsometric results for the construction of the spaced NP monolayer. The ellipsometric thickness of the spacer multilayer is 4.5 nm, in excellent agreement with the AFM profilometry shown in Figure 8b. The profilometry gives a value of 12.5 ± 1 nm for the total film thickness, as expected for the organic multilayer + NP monolayer.

The cross-sectional TEM image in Figure 9 shows a spaced NP layer "floating" on the TEM-invisible spacer (areas marked with arrows, inset). Apparent fluctuations in the spacing are attributed to slight misorientation of the slicing and Au substrate corrugation, as explained above. The largest observed spacing between the Au substrate and the NP layer is 3−4 nm (see inset in Figure 9), somewhat smaller than the expected spacing (4.5 nm). The deviation may be due to misorientation of the slicing, deformation of the sample by the section, or minor dimensional changes of the epoxy resin during curing.

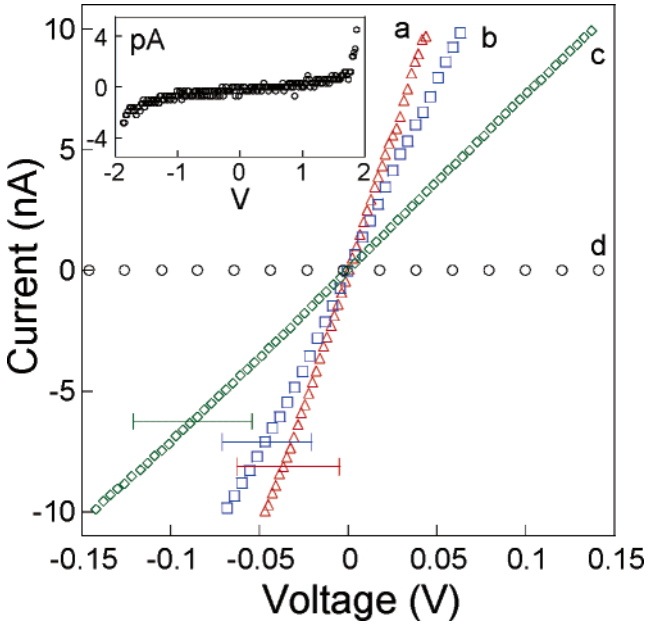

Figure 10. Conductive contact-mode AFM *I*−*V* curves obtained for 1 (a), 3 (b), and 6 (c) coordinated NP layers on Au substrates (bars show the standard deviation). (d) *I*−*V* curve for a NP layer constructed on a 4−5-nm coordinated multilayer spacer (as in Figure 9). Inset: Expanded view of *I*−*V* curve d (note the different current scale). Measurements were carried out in air.

Conductive AFM was used to investigate the electrical behavior of the NP films. Figure 10 shows typical current−voltage (I−V) curves (~30 measurement points on each sample) obtained for 1, 3, and 6 NP layers (parts a−c of Figure 10), as well as for a spaced NP layer (Figure 10d, same as in Figure 9). As seen in parts a−c of Figure 10, the NP films exhibit an ohmic response, similar to other reported systems at low voltages.[53,60] The measured resistance values are 1.9 ± 1.5, 3.2

± 1.9, and 12.5 ± 6.0 MΩ for 1, 3, and 6 NP layers, respectively. The relatively large variability is probably the result of different contact areas (i.e., number of contacted NPs) in different measurements. For the NP monolayer, occasional short circuits were encountered in certain measured points, apparently due to direct contact of the tip with the Au substrate at defects. The results show a clear increase in film resistance with the number of NP layers, i.e., with increased film thickness. The *I*−*V* curves in parts a−c of Figure 10 reproduce well for each point (i.e., second or third measurements). The electrical conductivity of NP films was previously studied by several groups, with values ranging from insulator to bulk gold, the discrepancies attributed mainly to interparticle distance.[53,60,61] The systematic increase in resistivity with the number of NP layers shown here emphasizes the role of the insulating organic capping layers in separating the NPs. A crude estimate, calculated by assuming a tip radius of 10 nm, gave specific resistivity values of 0.1−10 Ω cm for films a−c of Figure 10. These values, which are several orders of magnitude larger than the resistivity of bulk gold (2.4×10^{-6} Ω cm), are in agreement with the optical properties (Figure 4).

The *I*−*V* curve obtained for the spaced NP layer (Figure 10d and inset) is dramatically different. The measured resistance in the ohmic region is 10^5−10^6 MΩ, i.e., at least five orders of magnitude higher than the resistance of the NP layer coordinatively bound to the Au surface without the added spacer (Figure 10a). The *I*−*V* curves could be reproduced on the same point when currents smaller than 10−20 pA were allowed. In all measurements (parts a−d of Figure 10), there was virtually no force dependence of the current between 1 and 3 nN, implying negligible deformation or change in the contact area. The impressive insulating ability afforded by the 4−5-nm organic spacer clearly demonstrates the degree of molecular-scale control attainable with LbL coordination schemes. A more comprehensive study of the electrical behavior of the films requires additional (macroscopic) measurements and is currently underway.

Conclusions

Hydrophilic, hydroxyl-capped Au nanoparticles (NPs) were partially derivatized with bishydroxamate ligand molecules and used for coordination self-assembly of NP mono- and multilayers on evaporated, semitransparent Au substrates using Zr^{4+} as binding ions in a layer-by-layer (LbL) scheme. The NP layers were characterized by ellipsometry, wettability, transmission spectroscopy, AFM, and cross-sectional TEM imaging. The results show individual Au NPs forming a rather densely packed film, whose thickness increases regularly with the number of NP layers assembled. The coordinated NP films grow in a true LbL fashion, adding one NP monolayer at a time. This is analogous to the growth mode of similarly prepared coordinated organic multilayers[45] and is different from, e.g., Cu^{2+}/carboxylic acid NP films, where the growth of several interdigitated NP layers per adsorption step was observed. Formation of coordinated NP layers spaced from the Au substrate by a similarly coordinated organic multilayer demonstrated the possibility of constructing hybrid nanostructures comprising molecular and NP components, assembled using coordination chemistry and affording superior control over the structure. The structural properties of the films are reflected in their electrical properties, measured using conductive AFM, showing an ohmic resistance that increases with the number of NP layers and a much larger resistance induced by the organic multilayer spacer. The results show that coordination self-assembly is a convenient and versatile tool for the construction of composite nanostructures on surfaces, enabling the combination of different building blocks to form elaborate structures using the same chemistry.

Acknowledgment. Support from the Israel Science Foundation and the Minerva Foundation, Munich, is gratefully acknowledged. We thank Supratim Guha Ray for the use of the ellipsometry simulation program. M.W. is recipient of a Levy Eshkol Scholarship, Israel Ministry of Science. Bob Reuter of Molecular Imaging Company is gratefully acknowledged for helpful advice.

Supporting Information Available: XPS atomic concentrations of a SAM of **1** + Zr^{4+}, transmission spectra of a blank experiment with no Zr^{4+} binding, and complete refs 11, 46, 53, and 60. This material is available free of charge via the Internet at http://pubs.acs.org.

JA050016V

(60) Terrill, R. H.; et al. *J. Am. Chem. Soc.* **1995**, *117*, 12537−12548.
(61) Musick, M. D.; Keating, C. D.; Keefe, M. H.; Natan, M. J. *Chem. Mater.* **1997**, *9*, 1499−1501.